remote sensing

MDPI

Article

Dynamic Changes and Sediment Reduction Effect of Terraces on the Loess Plateau

Chenfeng Wang [1], Xiaoping Wang [2,*], Xudong Fu [3], Xiaoming Zhang [4] and Yunqi Wang [5]

[1] State Key Laboratory of Soil and Water Conservation and Desertification Control, College of Soil & Water Conservation Science and Engineering (Institute of Soil and Water Conservation), Northwest A&F University, Yangling, Xianyang 712100, China; chenfengwang@nwafu.edu.cn
[2] College of Natural Resources and Environment, Northwest A & F University, Yangling, Xianyang 712100, China
[3] State Key Laboratory of Hydroscience and Engineering, Tsinghua University, Beijing 100084, China; xdfu@tsinghua.edu.cn
[4] State Key Laboratory of Simulation and Regulation of Water Cycle in River Basin, China Institute of Water Resources and Hydropower Research, Beijing 100048, China; zhangxm@iwhr.com
[5] Three-Gorges Reservoir Area (Chongqing) Forest Ecosystem Research Station, School of Soil and Water Conservation, Beijing Forestry University, Beijing 100083, China; wangyunqi@bjfu.edu.cn
* Correspondence: wxp4911@nwafu.edu.cn

Highlights

What are the main findings?

- By combining remote sensing imaging principles with machine learning techniques, we produced 30 m terrace maps (1990–2020) for the Loess Platea, revealing significant spatiotemporal variations in terrace expansion.
- We quantified the sediment reduction resulting from terrace construction, revealing an average 49.75% decrease in soil erosion across the Loess Plateau.

What are the implications of the main findings?

- This study provides a robust framework for long-term monitoring of terrace dynamics, thereby offering a scientific basis for precision terrace management and sustainable land-use planning on the Loess Plateau.
- This study demonstrates the critical role of terrace engineering in soil and water conservation, providing quantitative evidence to support the optimization of erosion control and agricultural productivity strategies on the Loess Plateau.

Abstract

Terraces are the main engineering of soil erosion control on the Loess Plateau, offering measures for sediment reduction and water conservation, as well as the potential for increasing agricultural productivity. Over the years, large-scale terrace construction has been undertaken; however, the management has been inadequate, especially in terms of long-term monitoring and mapping. Moreover, the sediment reduction effect of terrace construction is not yet fully understood. Therefore, this study utilizes Landsat series data, integrating remote sensing imaging principles with machine learning techniques to achieve long–term temporal sequence mapping of terraces at a 30 m spatial resolution on the Loess Plateau. The sediment reduction effect brought about by terrace construction on the Loess Plateau is quantified using a sediment reduction formula. The results show that Elevation (Ele.), red band (R), Normalized Difference Vegetation Index (NDVI), Enhanced Vegetation Index (EVI), and Near-infrared Reflectance of Vegetation (NIRv) are key parameters for remote sensing identification of terraces. These five remote sensing variables explain 88% of

check for updates

Academic Editor: Lenio Soares Galvao

Received: 30 October 2025
Revised: 10 December 2025
Accepted: 10 December 2025
Published: 13 December 2025

Citation: Wang, C.; Wang, X.; Fu, X.; Zhang, X.; Wang, Y. Dynamic Changes and Sediment Reduction Effect of Terraces on the Loess Plateau. *Remote Sens.* **2025**, *17*, 4021. https://doi.org/10.3390/rs17244021

Copyright: © 2025 by the authors. Licensee MDPI, Basel, Switzerland. This article is an open access article distributed under the terms and conditions of the Creative Commons Attribution (CC BY) license (https://creativecommons.org/licenses/by/4.0/).

the terrace recognition variance. Coupling the Random Forest classification model with the LandTrendr algorithm allows for rapid time-series mapping of terrace spatial distribution characteristics on the Loess Plateau. The producer's accuracy of terrace identification is 93.49%, the user's accuracy is 93.81%, the overall accuracy is 88.61%, and the Kappa coefficient is 0.87. The LandTrendr algorithm effectively removes terraces affected by human activities. Terraces are mainly distributed in the southeastern Loess areas, including provinces such as Gansu, Shaanxi, and Ningxia. Over the past 30 years, the terrace area on the Loess Plateau has increased from 0.9790 million hectares in 1990 to 9.8981 million hectares in 2020. The sediment reduction effect is particularly notable, with an average reduction of 49.75% in soil erosion across the region. This indicates that terraces are a key measure for soil erosion control in the region and a critical strategy for improving farmland productivity. The data from this study provides scientific evidence for soil erosion control on the Loess Plateau and enhances the precision of terrace management.

Keywords: Loess Plateau; Random Forest classification model; terrace mapping; remote sensing identification; soil erosion; sediment reduction effect

1. Introduction

Loess Plateau is an important agricultural and soil conservation region in China [1,2]. However, its unique geographical and climatic conditions have long made the area prone to severe soil erosion issues [1,2]. To address this problem, terraces, as one of the main soil erosion control measures on the Loess Plateau, have been widely implemented in the region [3]. Terraces not only have significant effects on preventing soil erosion and conserving water, but they also improve soil quality and enhance agricultural production environments, thus holding potential for increasing crop yields [4]. Despite the extensive construction of terraces in the region, there are still numerous challenges in the management and monitoring of terraces, particularly in long-term monitoring and mapping, which remains insufficient.

Currently, the construction and management of terraces on the Loess Plateau continue to face many challenges, especially the lack of clear, quantitative assessments of the soil erosion reduction effect brought by terrace construction [5]. Traditional monitoring methods, such as field surveys and manual mapping, although providing accurate information for local areas, are costly, inefficient, and lack timeliness, making it difficult to achieve real-time monitoring of large-scale regions [6,7]. Therefore, remote sensing technology has become a crucial tool for large-scale, long-term monitoring and mapping of terraces. With its broad spatial coverage, high temporal resolution, and relatively low monitoring costs, remote sensing has become an essential tool in environmental monitoring [8,9]. Landsat series satellite data, one of the most widely used remote sensing data sources, has been extensively applied in land use/land cover change monitoring, vegetation change detection, and soil conservation effect assessments [10]. In addition, satellites such as ICESat-2 and Sentinel-1/2 are used for many studies on erosion, including river flow estimation [11]. Although the spatial resolution of multispectral data such as Sentinel-1/2 and GaoFen(GF) is superior to that of the Landsat series data, there is a lack of accumulation of long-term series data. Therefore, Landsat data is mainly selected for long-term and high-spatial resolution mapping.

Through the interpretation of remote sensing imagery, efficient mapping and spatiotemporal monitoring of terraces can be achieved. Additionally, with the rapid development of machine learning methods, especially in the processing of remote sensing data,

the accuracy of automated terrace recognition and classification has been significantly improved [12]. Machine learning algorithms can effectively extract spatial information from imagery and, by combining remote sensing data with environmental features, can accurately distinguish terraces from other land use types, enabling large-scale terrace mapping and monitoring [13]. With advancements in remote sensing technology and computer science, terrace extraction methods have evolved significantly from traditional spectral classification to automated recognition based on machine learning and deep learning techniques [14]. Early methods for terrace extraction mainly relied on the spectral characteristics of remote sensing imagery and employed traditional image classification algorithms (e.g., Maximum Likelihood Classification, Support Vector Machines, Decision Trees) to distinguish terraces from other land features [15]. However, due to the high spectral similarity between terraces and other agricultural or natural landscapes (e.g., grasslands, forests), these methods often face precision challenges in complex terrains or large-scale applications.

As an important soil conservation measure, the sediment reduction effect of terraces has become a research focus for many scholars. Several studies have shown that terrace construction can effectively reduce soil erosion, decrease sediment transport, and significantly improve the regional ecological environment [15,16]. Early studies mainly assessed the sediment reduction effect of terraces through field investigations and small-scale simulations. However, with the development of remote sensing technology, an increasing number of studies have adopted remote sensing imagery and models to estimate the sediment reduction effects on a large scale. Studies have found that the impact of terraces on soil conservation varies depending on the region and terrace design. Feng et al. [17] used a soil erosion model to assess the soil conservation benefits of terraces on the Loess Plateau. The results showed that terraces could reduce soil erosion by 39.08% and improve soil moisture retention [17]. On the other hand, Deng et al. [15] utilized soil erosion models to quantify the comprehensive benefits of terrace construction for soil conservation and agricultural production, finding that terraces not only help reduce soil loss but also promote vegetation cover and crop yield increases. Additionally, Chen et al. [16] performed a comparative analysis of soil erosion in terraces and natural landscapes, suggesting that the sediment reduction effect of terraces is not only dependent on terrain slope but also closely related to factors such as terrace scale, spacing, and soil properties. Therefore, optimizing terrace design to enhance its sediment reduction effect remains a key issue in current research.

Recently, with the complexity of climate change and human intervention, researchers have gradually focused on the long-term effects of terraces [18]. Tian et al. [18] interpreted the distribution of terraces in ArcGIS 10.7 using long-term remote sensing data and simplified method developed by Mekuriaw et al. [19]. They studied the changes in soil conservation effects of terraces on the Loess Plateau, finding that as terrace construction progressed, the soil erosion control gradually strengthened. However, excessive terracing may lead to land degradation and ecological damage. Thus, rational terrace management and design have become critical for achieving sustainable soil conservation. Terraces not only mitigate soil erosion in the short term but also have significant long-term effects on soil conservation. However, the spatial and temporal variations in the sediment reduction effect of terraces remain considerable. Therefore, quantifying the benefits of terraces and regional adaptation remains an important direction for future research.

This study aims to conduct terrace mapping on the Loess Plateau using Landsat series remote sensing data, combining remote sensing imaging principles with machine learning methods. It involves constructing a long-term time-series remote sensing imagery dataset, calculating the soil erosion reduction effect using a sediment reduction formula, and quantitatively evaluating the sediment reduction effects of terrace construction. The

data from this study will provide scientific evidence for soil erosion control on the Loess Plateau and improve the precision of terrace management.

2. Materials and Methods

2.1. Study Area

Loess Plateau is located in the middle reaches of the Yellow River (33°41′05″–41°16′06″N, 100°52′30″–114°33′02″E), spanning seven provincial-level administrative regions: Shaanxi, Shanxi, Gansu, Ningxia, Inner Mongolia, Henan, and Qinghai (Figure 1). The elevation ranges from 900 to 3000 m, with an annual average temperature between 2.4 and 14.2 °C as well as annual precipitation ranging from 300 to 650 mm. Precipitation is concentrated from July to September. The Loess Plateau is one of the most ecologically fragile regions in China [20]. Due to long-term natural erosion and unreasonable human activities, soil erosion has been a severe problem in this area. Soil erosion not only leads to a decline in land productivity but also exacerbates desertification, posing a significant threat to local ecological safety and sustainable development. To address soil erosion, the Gansu–Qinghai–Ningxia region has focused on terracing as a key project since 1997. As an effective soil and water conservation measure, terracing can significantly reduce soil erosion, improve soil fertility, and ensure the sustainable development of agriculture. Through terracing, the ecological environment in this region has been partially optimized [21].

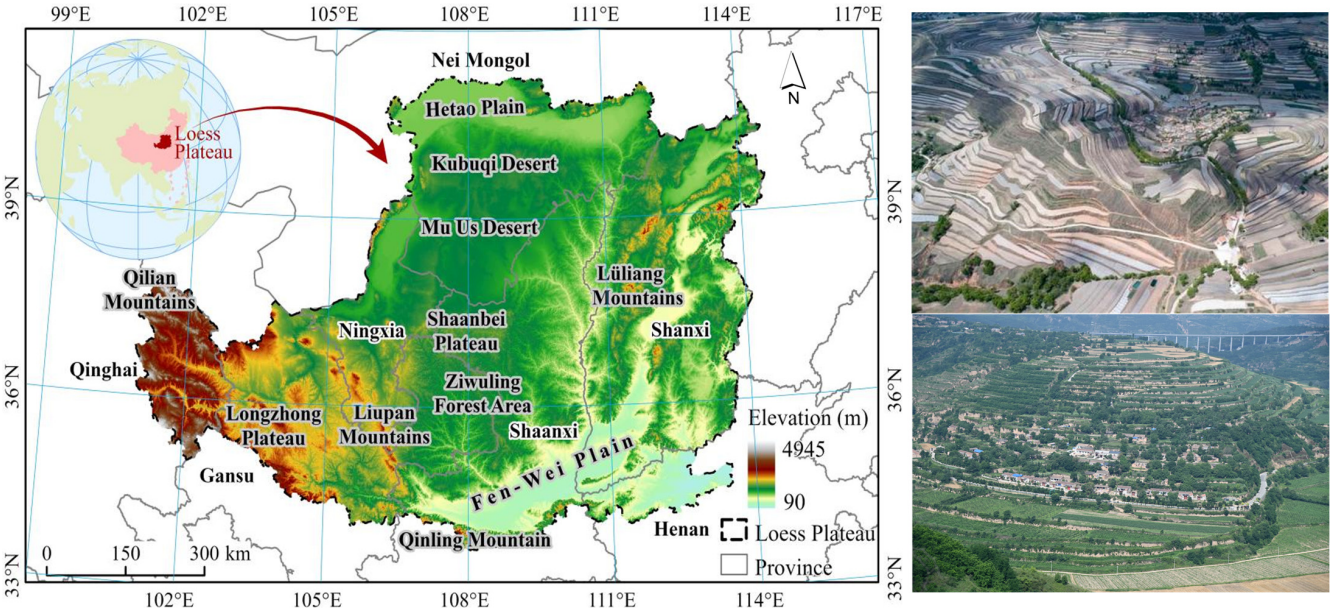

Figure 1. Location of the Loess Plateau.

2.2. Data Sources

2.2.1. Landsat Imagery

Landsat imagery used in this study includes surface reflectance (SR) data from Landsat Level 1 (highest quality). The data product has been geometrically, radiometrically, and atmospherically corrected, with a spatial resolution of 30 m and a temporal resolution of 16 days. The data primarily consist of images from Landsat 5 (Thematic Mapper, TM), Landsat 7 (Enhanced Thematic Mapper Plus, ETM+), and Landsat 8 (Operational Land Imager, OLI). Due to the different service lifespans of Landsat 5/7/8 satellites, Landsat 5 imagery was used from 1988 to 2011, Landsat 7 for 2012, and Landsat 8 for 2013–2020, with a total of 1690 scenes of imagery.

2.2.2. Sample Data

Land cover was classified into two categories: terraced fields and other land types. Sample data were collected through visual interpretation of historical high-resolution imagery from Google Earth Pro, comprising both point samples and patch (area) samples, each designed for a specific validation purpose. Point samples were collected based on two principles: (1) a 5 km grid was overlaid on the study area to ensure spatial uniformity, and (2) points representing the same land cover class were kept within 100 m of each other. A total of 2673 points were obtained (1040 for terraced fields, 1633 for other types). These points were used for pixel-level classification training and accuracy assessment of the satellite imagery (Landsat 5/7/8). Patch samples consisted of six randomly distributed 5 km × 5 km regions, which were manually digitized from 2019 Google Earth imagery and verified by field survey. These continuous reference areas were used to visually evaluate the spatial consistency and boundary accuracy of the classification results over larger contiguous landscapes, complementing the point-based statistical validation.

2.2.3. Slope Data Based on DEM

DEM data (Copernicus DEM, COP DEM) used in this study was released by the European Space Agency (ESA). It is recognized as one of the best open-source DEMs, with excellent terrain detail, absolute elevation accuracy, and horizontal precision, among the best of any global open-source DEM. Therefore, we selected the COP DEM for 2015 as the terrain data source. This data was downloaded from the ESA website (https://www.esa.int/), with a spatial resolution of 30 m and projected in UTM/WGS84. The slope was calculated using ArcGIS Pro (v3.4.2).

2.3. Methods

The dynamic monitoring of Loess Plateau terraces follows a four-step process: (1) Remote sensing data preparation, which includes Landsat reflectance data (Landsat SR), DEM, and sample data. (2) The data preprocessing stage comprised four key steps. First, multi-scene images were mosaicked to ensure complete coverage of the study area. Second, spectral indices (listed in Table 1) were calculated to enhance features relevant to terrace identification. Third, clouds and their shadows were detected and masked using an algorithm to minimize atmospheric interference. Finally, slope information was derived from the digital elevation model (DEM). (3) Model training and terrace identification. (4) Time-series result optimization. The dynamic monitoring process of Loess Plateau terraces is illustrated in Figure 2.

Table 1. Spectral index calculation methods.

Spectral Index	Abbreviation	Equation	Reference
Normalized Difference Vegetation index	NDVI	$(NIR - R)/(NIR + R)$	[22]
Enhanced Vegetation Index	EVI	$2.5 \times (NIR - R)/(NIR + 6 \times R - 0.75 \times B + 1)$	[23]
Normalized Difference Built-up Index	NDBI	$(SWIR - NIR)/(SWIR + NIR)$	[24]
Normalized Difference Moisture Index	NDMI	$(NIR - SWIR)/(NIR + SWIR)$	[25]
Normalized Difference Water Index	NDWI	$(G - NIR)/(G + NIR)$	[26]
Near-infrared Reflectance of Vegetation	NIRv	$(NIR - R)/(NIR + R) \times NIR$	[27]

Note: NIR represents near-infrared reflectance, R represents red band reflectance, B represents blue band reflectance, SWIR represents shortwave-infrared reflectance, G represents green band reflectance.

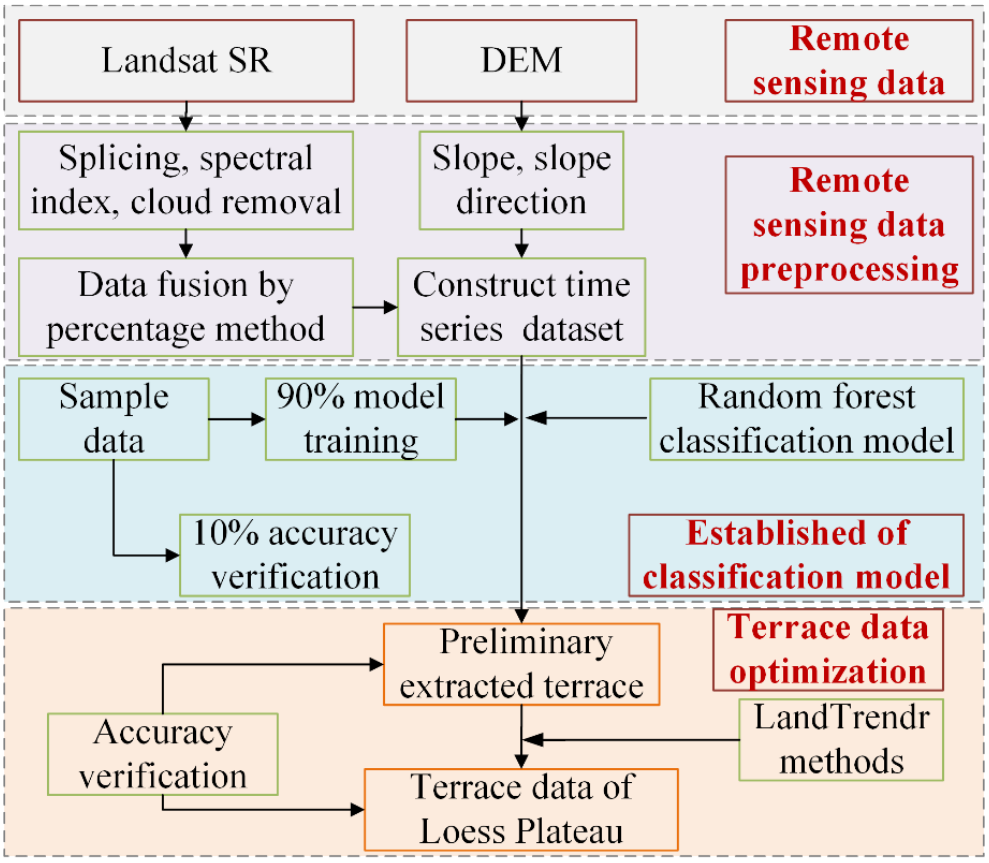

Figure 2. Technical flowchart of dynamic monitoring of Loess Plateau terraces.

2.3.1. Spectral Index Selection

The spectral bands used for Landsat imagery include the red band (R), green band (G), blue band (B), near–infrared band (NIR), shortwave-infrared band 1 (SWIR1), and shortwave-infrared band 2 (SWIR2). After trimming (removing bad pixels), spectral indices were calculated (method outlined in Table 1) and cloud removal was performed. For the Loess Plateau terraces, considering the seasonal changes throughout the year, the 10%, 25%, 50%, 75%, and 90% percentiles of the time-series data were calculated for each pixel in each spectral band. These percentiles were used to generate five corresponding band indices for each pixel. These indices were then combined with six terrain feature bands, including elevation, slope, aspect, and three terrain roughness bands calculated from 3×3, 7×7, and 11×11 pixel windows, totaling 61 feature bands.

2.3.2. Machine Learning

Random Forest is a decision tree method based on Bagging, with a core principle of using the Bagging algorithm and randomly selecting features. Given a training set, the Bagging algorithm generates multiple subsets by random sampling with replacement, and decision trees are trained on these subsets [28]. Finally, the results of the decision trees are averaged or majority-voted to produce the final classification. Additionally, during each candidate split, Random Forest randomly selects a subset of features, further increasing the diversity and generalization ability of the model. In machine learning, the sample data are mapped annually to the corresponding composite images (e.g., Landsat 5 samples for 2000, 2010, and 2011) and then split into a 90:10 ratio for training and accuracy validation.

2.3.3. Calculation of Feature Importance

Feature importance is calculated by averaging the contribution of each feature and comparing them. Typically, the out-of-bag (OOB) error rate is used to assist in feature selection. The calculation formula is as follows [29]:

$$FIM_i = \frac{\sum errOOB_2 - errOOB_1}{N} \quad (1)$$

where *FIM* is the feature importance score, *i* is the feature index, *N* is the number of decision trees, and $errOOB_1$ is the normal out-of-bag error, which indicates the standard out-of-bag error calculated from the original training dataset and serves as the baseline metric for model performance. $errOOB_2$ is the out-of-bag error with noise interference, representing the error after introducing controllable noise interference to the input features. That is, pixels are randomly selected in each feature layer and random Gaussian noise with a mean of 0 and a standard deviation of 0.1 to 10% is added. This noise injection simulates potential data perturbations to evaluate the robustness of the model.

2.3.4. LandTrendr Algorithm and Result Optimization

LandTrendr algorithm segments the time series by year, fits and smooths each segment, and captures the overall change characteristics of each pixel over the study period [30]. To reduce errors caused by extreme weather or human activities, the LandTrendr algorithm is used to smooth the time series results (probabilities ranging from 0 to 1), leveraging the stable temporal characteristics of land cover types.

2.3.5. Accuracy Analysis

Based on the sample points, the confusion matrix calculates the overall accuracy (*OA*), producer's accuracy (*PA*), and user's accuracy (*UA*). The classification thresholds for each land cover type were determined based on these accuracy metrics. The calculation formulas for overall accuracy, producer's accuracy, and user's accuracy are as follows [31]:

$$OA = \frac{n}{M} \quad (2)$$

$$PA = \frac{n}{N} \quad (3)$$

$$UA = \frac{n}{n+k} \quad (4)$$

where *n* represents the number of correctly classified samples, *N* is the number of samples in that category, *M* is the total number of samples, and *k* is the number of samples misclassified into that category.

In addition, to accurately evaluate the algorithm, this paper adopts recall rate and *F*1 score as evaluation indicators. The recall rate (*Re*) is used to calculate the percentage of correctly predicted step pixels to the actual steps. The *F*1 score is the sum of the above two and can reflect the overall predictive ability of the model. The specific calculation formula is as follows:

$$Re = \frac{TP}{TP + FN} \quad (5)$$

$$F1 = \frac{2PR}{P + R} \quad (6)$$

$$P = \frac{TP}{TP + FP} \quad (7)$$

where *R* represents the recall rate; *F*1 is the *F*1 score; *P* is the precision. *TP* denotes the number of positive samples predicted to be positive (true positive). *FP* denotes the

number of negative samples predicted as positive. *TN* denotes the number of negative samples predicted to be negative. *FN* denotes the number of positive samples predicted to be negative.

2.4. Terrace Sediment Reduction Effect Analysis

Recently, Liu et al. [32] established a relationship between terrace ratio and sediment reduction magnitude based on measured sediment load data from hydrological stations on the Loess Plateau:

$$W_s = 100 - \frac{100}{1 + \left(\frac{T_i}{14}\right)^{2.35}} \quad (8)$$

where W_s is the sediment reduction magnitude (%), and T_i is the terrace ratio (%), representing the proportion of terrace area to the area with slight or more severe soil erosion in a certain region. This model not only reflects the sediment reduction effect of the terraces themselves but also their contribution to sediment reduction in the upper and lower parts of the basin at a watershed.

3. Results

3.1. Model Parameter Construction and Accuracy Evaluation

3.1.1. Feature Importance

Feature selection is one of the important steps in building a machine learning model, aiming to reduce the input features of the model by using relevant features and eliminating noise in the dataset. In model construction, selecting relevant features directly affects the model's accuracy and complexity. In this study, 14 feature variables, including band reflectance, surface reflectance, and elevation, were input into the model to analyze feature importance. The results are shown in Figure 3. The top five model variables ranked from highest to lowest are as follows: Elevation (Ele.) > Red band (R) > NDVI > EVI > NIRv. These top five variables contribute approximately 88% to terrace identification. We found that, in terrace recognition, key parameters include elevation, red band spectral reflectance, NDVI, EVI, and NIRv indices.

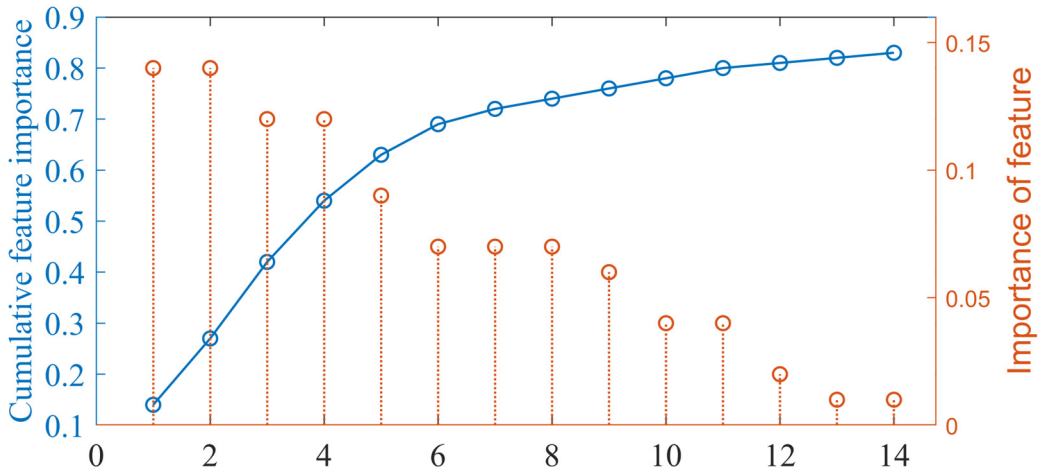

Figure 3. Importance of feature and cumulative feature importance.

3.1.2. Accuracy Evaluation

Table 2 shows the validation results for 1051 randomly selected sample points with four accuracy indicators. The results indicate that the accuracy based on the sample point verification for the Random Forest algorithm is as follows: producer's accuracy for terraces: 93.49%, user's accuracy for terraces: 93.81%, overall accuracy: 88.61%, and Kappa

coefficient: 0.87. At the same time, the accuracy rate and recall rate *F*1 scores were used for progress comparison, and it was found that these results met the basic requirements of remote sensing land cover classification.

Based on remote sensing recognition and processed by the LandTrendr algorithm, the terrace area in the study area is shown in Figure 4. On the left side of Figure 4, there is a high-resolution Google Earth image, a Landsat OLI image in the middle, and the recognition results on the right. We observe that remote sensing images alone cannot visually identify the spatial features of terraces. The recognition can only rely on spectral features and spectral indices of land cover, further confirming that land cover spectral characteristics in remote sensing data are essential variables for recognizing large-area terraces. After processing with the LandTrendr algorithm, human activity disturbances (such as abandoned terraces) are clearly identified, and only the terraces that need to be utilized are extracted.

Table 2. Sample points verification accuracy of the results.

Year	PA (%)	OA (%)	UA (%)	Kappa	*P*	*Re*	*F*1
1990	93.23	88.02	94.01	0.88	0.81	0.74	0.77
2000	93.13	87.92	93.91	0.86	0.82	0.72	0.76
2010	92.37	87.35	92.98	0.82	0.86	0.78	0.82
2020	95.21	91.12	94.32	0.90	0.87	0.83	0.85
Mean	93.49	88.61	93.81	0.87	0.84	0.76	0.80

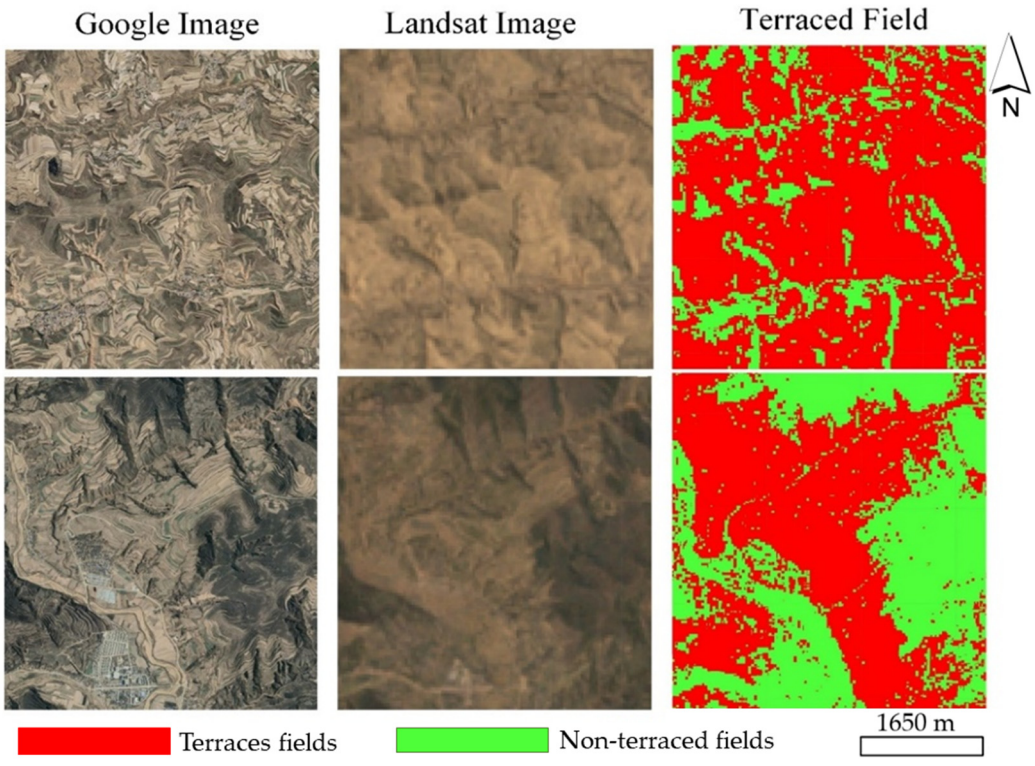

Figure 4. LandTrendr algorithm-optimized terrace features of the Loess Plateau.

3.2. Terrace Area Change Trends over the Past 30 Years

From 1990 to 2020, in terms of the overall distribution of terraces on the Loess Plateau (Figure 5), terraces are mainly concentrated in the southeastern Loess region, which spans core areas such as Gansu, Shaanxi, and Ningxia. These regions are part of the Loess Plateau's central zone, characterized by complex terrain, with numerous gullies and severe soil erosion. Geographically, terraces are widely distributed in hilly and gully regions.

These areas have significant terrain undulation and steep slopes. However, terracing is mostly carried out along contour lines, effectively reducing soil erosion.

Overall, from 1990 to 2020, the terrace area on the Loess Plateau showed an increasing trend, from 0.9790 million hectares in 1990 to 9.8981 million hectares in 2020 (in Figure 6). However, regional differences in changes are significant. In Gansu Province, there was a sharp increase from 1.8617 million hectares in 2010 to 4.5546 million hectares in 2020, while other regions showed slower changes. In Shanxi, the area increased from 0.2068 million hectares in 1980 to 1.7827 million hectares in 2020.

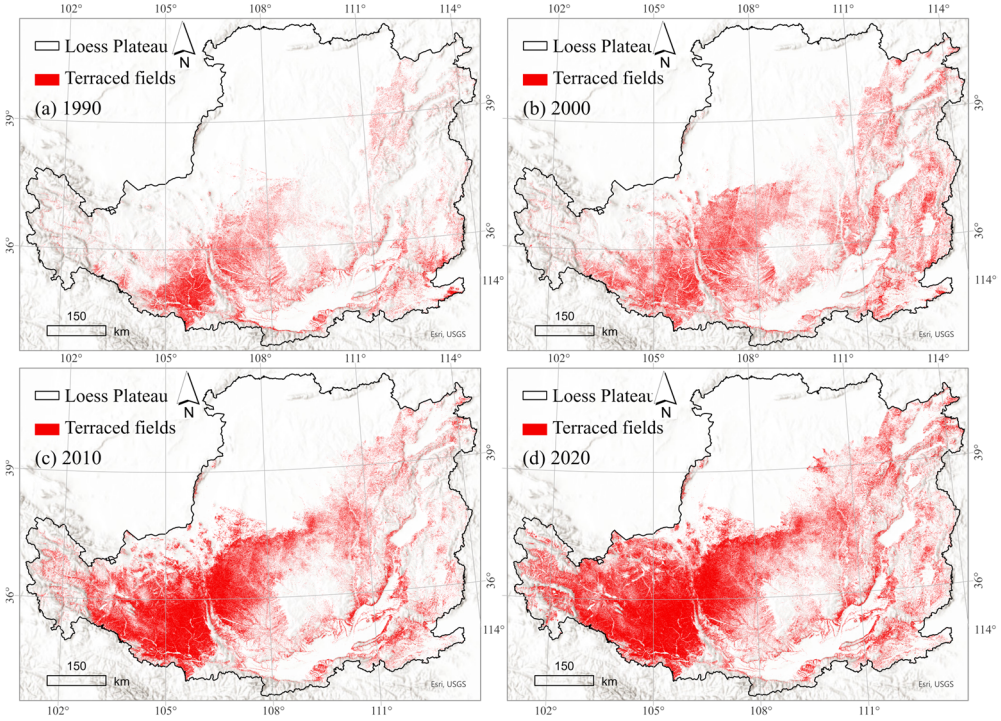

Figure 5. Spatial changes in terraces on the Loess Plateau.

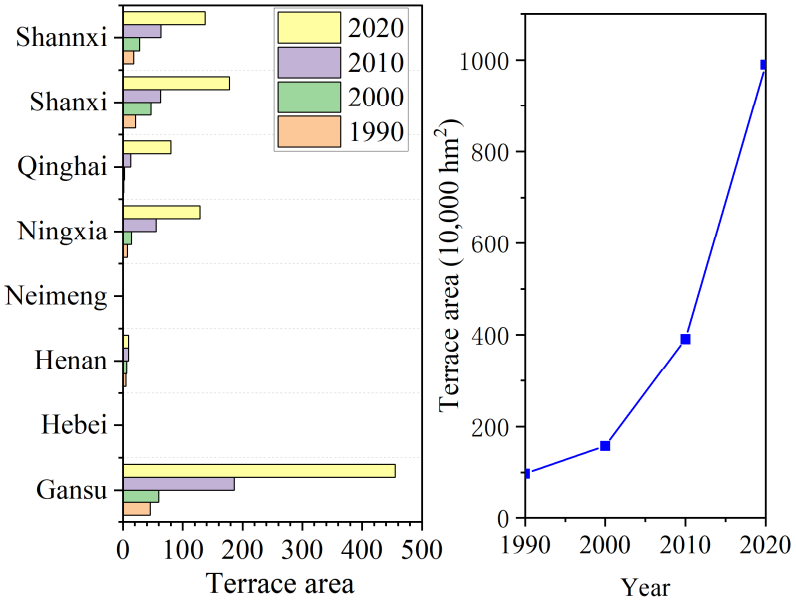

Figure 6. Temporal changes in terraces on the Loess Plateau.

3.3. Sediment Reduction Effect of Terraces on the Loess Plateau over the Past 30 Years

From 1990 to 2020, the terrace area on the Loess Plateau substantially increased (Figure 7), which greatly reduced soil erosion. The average sediment reduction across the region was 49.75%. In 1990, with an average terrace area of 0.9790 million hectares, the average sediment reduction was 45%. In 2000, with 1.5790 million hectares of terraces, the average sediment reduction was 49%. In 2010, 3.9071 million hectares of terraces led to an average sediment reduction of 50%, and in 2020, the sediment reduction reached 55% with 9.8981 million hectares of terraces.

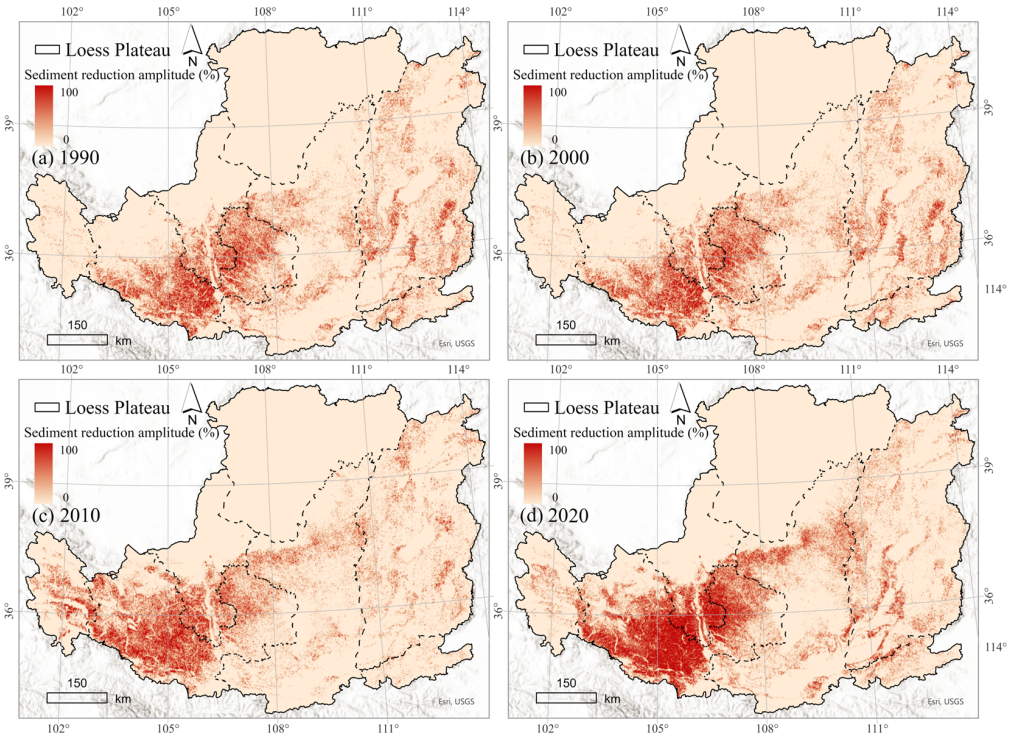

Figure 7. Spatial sediment reduction effect of terraces on the Loess Plateau.

4. Discussion

In this study, we investigated for the first time the long-term dynamics of terrace coverage on the Loess Plateau by integrating multi-decadal Landsat imagery with a Random Forest and LandTrendr framework. This novel methodology enables annual, high-accuracy mapping (OA: 88.61%, Kappa: 0.87) and distinguishes stable terraces from recent changes. Our results provide the first 30-year, spatially explicit quantification, revealing terrace expansion from 0.98 to 9.90 million hectares (1990–2020) and linking it to a substantial regional sediment reduction effect (average 49.75%). This work offers both a transferable monitoring workflow and critical evidence for assessing long-term soil and water conservation efficacy.

4.1. Uncertainty in Long-Term Terrace Monitoring Methods

Remote sensing technology provides an effective means for long-term monitoring of terraces. Landsat series satellite data, with its high spatial resolution and temporal continuity, has become an important data source for monitoring terraces on the Loess Plateau. Studies have shown that remote sensing imagery can accurately extract the spatial distribution and changes in terraces, enabling dynamic monitoring of terraces [33]. Especially in the complex terrain of the Loess Plateau, traditional field survey methods are difficult to meet the demands of frequency monitoring. Remote sensing technology clearly provides a more efficient and cost-effective alternative. Furthermore, with the introduction of deep learning and machine learning methods, the automation and accuracy of terrace

extraction have been significantly improved. Deep learning models, such as Convolutional Neural Networks (CNNs) and U–Net, can automatically identify and classify terraces from remote sensing images, particularly demonstrating strong advantages in long–term data processing [34].

However, despite the improvement in the accuracy of terrace extraction through machine learning methods, there are still challenges. Particularly in the application of high-resolution remote sensing imagery, terraces often share similar spectral characteristics with other land cover types (such as farmland or grasslands), which can lead to classification errors. Therefore, not only the basic characteristics of land use should be considered, but also many factors such as soil properties should be taken into account to improve the accuracy of remote sensing extraction of terraced fields.

4.2. Key Findings on Terrace Expansion and Its Environmental Efficacy

This study provides the first systematic quantification of the spatiotemporal evolution and major environmental benefits of terraced fields on the Loess Plateau from 1990 to 2020. The empirical results show that the area of terraced fields expanded explosively—from 979,000 hectares to 9.8981 million hectares—an increase of more than ninefold. In particular, rapid expansion occurred after 2010 in core regions such as Gansu, consistent with survey-based findings [35]. Spatially, terraced fields are highly concentrated in the southeastern gully regions of the Loess Plateau, aligning closely with areas suffering from severe soil erosion [36].

By integrating an empirical modeling framework, this study is also the first to quantitatively assess the sediment reduction benefits of terracing using long-term remote sensing observations. Results indicate that terraced field construction contributed an average of approximately 49.75% to soil erosion reduction over the past three decades, reaching as high as 55% in 2020. These findings not only verify the intensity of large-scale ecological restoration efforts but also establish a direct quantitative link between terraced field construction and sediment reduction [37], providing robust empirical evidence for evaluating the effectiveness of soil and water conservation policies.

4.3. Uncertainty in Quantitative Study of Terrace Sediment Reduction Effects

The quantitative study of terrace sediment reduction effects in this research adopts a sediment reduction formula developed by Liu et al. [32]. The above sediment reduction formula was an empirical relationship established using terrace ratio and sediment data from hydrology stations in the upper reaches of the Wei River and the Zuli River. Since the sediment reduction effect of terraces is closely related to various factors (such as terrace design, soil type, vegetation cover, etc.), its effect varies in different regions and environmental conditions. As a result, existing studies mainly rely on remote sensing data and soil erosion models to assess the sediment reduction effect of terraces. Tian et al. [18] detected 4.73×10^4 km^2 of terraces by 2018, which covered approximately 1.5% of the whole Loess Plateau. The terraces were mainly distributed in the upstream of the Weihe River, Fenhe, Zuli, Jinghe, and Taohe River basins. The validated soil erosion model showed that vegetation changes caused a remarkable reduction of 51.2% soil erosion from 2000 to 2018 across the Loess Plateau. A scenario modeling with terraces reduced 19.4% of soil erosion, indicating their significant effects on soil erosion control [18]. However, the applicability of this result still needs further verification, as the sediment reduction effect may differ significantly under varying topographic and climatic conditions [37]. Therefore, optimizing terrace design and management strategies to enhance their sediment reduction benefits is crucial for promoting sustainable soil and water conservation and agricultural production in the Loess Plateau region.

5. Conclusions

This study utilizes Landsat series data, considers remote sensing imaging methods, and integrates machine learning methods to achieve long-term (1990–2020) terrace mapping on the Loess Plateau. It further analyzes the sediment reduction effects of terrace construction on the Loess Plateau. The main conclusions are as follows:

(1) Elevation (Ele.), Red band (R), Normalized Difference Vegetation Index (NDVI), Enhanced Vegetation Index (EVI), and NIRv are the key parameters for remote sensing identification of terraces. These five remote sensing variables can explain 88% of the terrace identification variables. Additionally, coupling the Random Forest classification model with the LandTrendr algorithm enables fast time-series mapping of terrace spatial distribution characteristics on the Loess Plateau. The producer's accuracy for terrace identification is 93.49%, user's accuracy is 93.81%, overall accuracy is 88.61%, and the Kappa coefficient is 0.87. The LandTrendr algorithm effectively removes terraces impacted by human activities.

(2) Terraces are mainly distributed in the Loess regions of the southeastern part of the plateau, including provinces such as Gansu, Shaanxi, and Ningxia. Between 1990 and 2020, the overall area of terraces showed an increasing trend, from 0.979 million hectares in 1990 to 9.8981 million hectares in 2020. However, the changes vary significantly across different provinces. For example, in Gansu Province, the area increased dramatically between 2010 and 2020, from 1.8617 million hectares in 2010 to 4.5546 million hectares in 2020.

(3) The average sediment reduction across the region is 49.75%, demonstrating that terraces are a key measure for regional soil and water conservation and a crucial approach to enhancing the quality and productivity of arable land. The data provided by this study offers scientific evidence for soil erosion control in the Loess Plateau region and improves the precision of terrace management.

Author Contributions: Conceptualization, C.W. and X.W.; data curation, X.W. and C.W.; formal analysis, C.W. and X.W.; funding acquisition, C.W., X.W., X.F. and X.Z.; investigation, C.W., X.Z. and Y.W.; methodology, C.W. and X.W.; project administration, C.W., X.W., X.F. and X.Z.; resources, C.W. and X.W.; software, C.W. and X.W.; supervision, C.W.; validation, C.W. and X.W.; visualization, C.W.; writing—original draft, C.W. and X.W.; writing—review and editing, C.W., X.W., X.F., X.Z. and Y.W. All authors have read and agreed to the published version of the manuscript.

Funding: This study was funded by the National Natural Science Foundation of China (U2243240, 42207396), the National Key Research and Development Program of China (2022YFE0115300, 2022YFF1300801).

Data Availability Statement: The Sentinel-1 SAR imagery and associated metadata are available on https://search.asf.alaska.edu/ (accessed on 10 December 2023). The Landsat-9 pan-sharpened tiled imagery service is provided by ©ESRI ArcGIS Online service (https://www.arcgis.com/home/item.html?id=a7412d0c33be4de698ad981c8ba471e6, accessed on 10 December 2023)). The ASTER GDEM V3 is available on www.earthdata.nasa.gov (accessed on 10 December 2023).

Conflicts of Interest: The authors declare no conflicts of interest.

References

1. Dorren, L.; Rey, F. A review of the effect of terracing on erosion. In *Briefing Papers of the 2nd Scape Workshop*; Boix-Fayons, C., Imeson, A., Eds.; SCAPE: Cinque Terre, Italy, 2004; pp. 97–108.
2. Hammad, A.H.A.; Brresen, T.; Haugen, L.E. Effects of rain characteristics and terracing on runoff and erosion under the Mediterranean. *Soil Tillage Res.* **2006**, *87*, 39–47. [CrossRef]
3. Yu, M.G.; Rui, X.P.; Xie, W.Y.; Xu, X.J.; Wei, W. Research on automatic identification method of terraces on the Loess Plateau Based on deep transfer learning. *Remote Sens.* **2022**, *14*, 2446. [CrossRef]

4. Pijl, A.; Wang, W.D.; Straffelini, E.; Tarolli, P. Soil and water conservation in terraced and non–terraced cultivations—A massive comparison of 50 vineyards. *Land Degrad. Dev.* **2021**, *33*, 596–610. [CrossRef]
5. Zhang, X.P.; Zhang, L.; Zhao, J.; Rustomji, P.; Hairsine, P. Responses of streamflow to changes in climate and land use/cover in the Loess Plateau, China. *Water Resour. Res.* **2008**, *44*, 1–12. [CrossRef]
6. Wang, S.; Fu, B.J.; Piao, S.L.; Lü, Y.H.; Ciais, P.; Feng, X.M.; Wang, Y.F. Reduced sediment transport in the Yellow River due to anthropogenic changes. *Nat. Geosci.* **2016**, *9*, 38–41. [CrossRef]
7. Xiong, L.Y.; Tang, G.A.; Yang, X.; Li, F.Y. Geomorphology–oriented digital terrain analysis: Progress and perspectives. *J. Geogr. Sci.* **2021**, *76*, 595–611. (In Chinese) [CrossRef]
8. Zhao, H.Q.; Fang, X.; Ding, H.; Josef, S.; Xiong, L.Y.; Na, J.M.; Tang, G.A. Extraction of terraces on the Loess Plateau from high–resolution dems and imagery utilizing object–based image analysis. *ISPRS Int. J. Geo-Inf.* **2017**, *6*, 157. [CrossRef]
9. Pijl, A.; Quarella, E.; Vogel, T.A.; D'Agostino, V.; Tarolli, P. Remote sensing vs. field–based monitoring of agricultural terrace degradation. *Int. Soil Water Conserv. Res.* **2021**, *9*, 1–10. [CrossRef]
10. Han, Q.; Yu, X.X.; Wang, W.; Xu, M.M.; Ren, R.; Zhang, J.P. Effect of terracing project on temporal–spatial variation of non–point source pollution load in Hujiashan watershed, China. *Chin. J. Appl. Ecol.* **2017**, *28*, 1344–1351. (In Chinese)
11. Liu, Q.; Chen, Y.; Brêda, J.P.L.; Cui, H.; Duan, H.; Huang, C. Higher-density river discharge observation through integration of multiple satellite data: Midstream yellow river, china. *Int. J. Appl. Earth Obs. Geoinf.* **2025**, *137*, 104433. [CrossRef]
12. Martínez–Casasnovas, J.A.; Ramos, M.C.; Cots–Folch, R. Influence of the EU CAP on terrain morphology and vineyard cultivation in the Priorat region of NE Spain. *Land Use Policy* **2010**, *27*, 11–21. [CrossRef]
13. Agnoletti, M.; Cargnello, G.; Gardin, L.; Santoro, A.; Bazzoffi, P.; Sansone, L.; Pezza, L.; Belfiore, N. Traditional landscape and rural development: Comparative study in three terraced areas in northern, central and southern Italy to evaluate the efficacy of GAEC standard 4.4 of cross compliance. *Ital. J. Agron.* **2011**, *6*, 121–139. [CrossRef]
14. Zhao, B.Y.; Ma, N.; Yang, J.; Li, Z.H.; Wang, Q.X. Extracting features of soil and water conservation measures from remote sensing images of different resolution levels: Accuracy analysis. *Bull. Soil Water Conserv.* **2012**, *32*, 154–157. (In Chinese)
15. Deng, C.X.; Zhang, G.Y.; Liu, Y.J.; Nie, X.D.; Li, Z.W.; Liu, J.Y.; Zhu, D.M. Advantages and disadvantages of terracing: A comprehensive review. *Int. Soil Water Conse. Res.* **2021**, *9*, 344–359. [CrossRef]
16. Chen, D.; Wei, W.; Chen, L. Effects of terracing practices on water erosion control in China: A meta-analysis. *Earth-Sci. Rev.* **2017**, *173*, 109–121. [CrossRef]
17. Feng, J.; Wei, W.; Pan, D.L. Effects of rainfall and terracing-vegetation combinations on water erosion in a loess hilly area, China. *J. Environ. Manag.* **2020**, *261*, 110247. [CrossRef] [PubMed]
18. Tian, P.; Tian, X.J.; Geng, R.; Zhao, G.J.; Yang, L.; Mu, X.M.; Gao, P.; Sun, W.Y.; Liu, Y.L. Response of soil erosion to vegetation restoration and terracing on the Loess Plateau. *Catena* **2023**, *227*, 107103. [CrossRef]
19. Mekuriaw, A.; Heinimann, A.; Zeleke, G.; Hurni, H.; Hurni, K. An automated method for mapping physical soil and water conservation structures on cultivated land using GIS and remote sensing techniques. *J. Geog. Sci.* **2017**, *27*, 79–94. [CrossRef]
20. Wang, K.L.; Zhou, J.; Tan, M.L.; Lu, P.D.; Xue, Z.H.; Liu, M.Y.; Wang, X.P. Impacts of vegetation restoration on soil erosion in the Yellow River Basin, China. *Catena* **2024**, *234*, 107547. [CrossRef]
21. Liu, X.H.; He, B.L.; Li, Z.X.; Zhang, J.L.; Wang, L.; Wang, Z. Influence of land terracing on agricultural and ecological environment in the loess plateau regions of China. *Environ. Earth Sci.* **2011**, *62*, 797–807. [CrossRef]
22. Fensholt, R.; Sandholt, I.; Rasmussen, M.S. Evaluation of MODIS LAI, fAPAR and the relation between fAPAR and NDVI in a semi–arid environment using in situ measurements. *Remote Sens. Environ.* **2004**, *91*, 490–507. [CrossRef]
23. Sakamoto, T.; Yokozawa, M.; Toritani, H.; Shibayama, M.; Ishitsuka, N.; Ohno, H. A crop phenology detection method using time–series MODIS data. *Remote Sens. Environ.* **2005**, *96*, 366–374. [CrossRef]
24. Haboudane, D.; Miller, J.R.; Pattey, E.; Zarco-Tejada, P.J.; Strachan, I.B. Hyperspectral vegetation indices and novel algorithms for predicting green LAI of crop canopies: Modeling and validation in the context of precision agriculture. *Remote Sens. Environ.* **2004**, *90*, 337–352. [CrossRef]
25. Jackson, T.J.; Chen, D.Y.; Cosh, M.; Li, F.Q.; Anderson, M.; Walthall, C.; Doriaswamy, P.; Hunt, E.R. Vegetation water content mapping using Landsat data derived normalized difference water index for corn and soybeans. *Remote Sens. Environ.* **2004**, *92*, 475–482. [CrossRef]
26. McFEETERS, S.K. The use of the Normalized Difference Water Index (NDWI) in the delineation of open water features. *Int. J. Remote Sens.* **1996**, *17*, 1425–1432. [CrossRef]
27. Wan, L.; Ryu, Y.; Dechant, B.; Hwang, Y.; Feng, H.; Kang, Y.H.; Jeong, S.; Lee, J.; Choi, C.; Bae, J. Correcting confounding canopy structure, biochemistry and soil background effects improves leaf area index estimates across diverse ecosystems from Sentinel–2 imagery. *Remote Sens. Environ.* **2024**, *309*, 114224. [CrossRef]
28. Briem, G.J.; Benediktsson, J.A.; Sveinsson, J.R. Multiple classifiers applied to multisource remote sensing data. *IEEE Trans. Geosci. Remote. Sens.* **2002**, *40*, 2291–2299. [CrossRef]

29. Stefanski, J.; Mack, B.; Björn, W. Optimization of object–based image analysis with random forests for land cover mapping. *IEEE J. Sel. Top. Appl. Earth Obs. Remote Sens.* **2013**, *6*, 2492–2504. [CrossRef]
30. Kennedy, R.E.; Yang, Z.Q.; Cohen, W.B. Detecting trends in forest disturbance and recovery using yearly Landsat time series: 1. LandTrendr–Temporal segmentation algorithms. *Remote Sens. Environ.* **2010**, *114*, 2897–2910. [CrossRef]
31. Zhen, Z.; Quackenbush, L.J.; Stehman, S.V.; Zhang, L.J. Impact of training and validation sample selection on classification accuracy and accuracy assessment when using reference polygons in object–based classification. *Int. J. Remote Sens.* **2013**, *34*, 6914–6930. [CrossRef]
32. Liu, X.Y.; Yang, S.T.; Wang, F.G.; He, X.Z.; Ma, H.B.; Luo, Y. Analysis on sediment yield reduced by current terrace and shrubs–Herbs–Arbor Vegetation in the Loess Plateau. *J. Hydraul. Eng.* **2014**, *45*, 1293–1300. (In Chinese)
33. Lu, D.; Su, K.C.; Wang, Z.P.; Hou, M.J.; Li, X.X.; Lin, A.W.; Yang, Q.Y. Patterns and drivers of terrace abandonment in China: Monitoring based on multi-source remote sensing data. *Land Use Policy* **2025**, *148*, 107388. [CrossRef]
34. Zhang, Y.; Shi, M.C.; Zhao, X.; Wang, X.J.; Luo, Z.D.; Zhao, Y. Methods for automatic identification and extraction of terraces from high spatial resolution satellite data (China-GF-1). *Int. Soil Water Conse. Res.* **2017**, *5*, 17–25. [CrossRef]
35. Zhang, Y.; Guo, X.F.; Han, J.Q.; Sun, P.C. Preliminary estimation of soil carbon sequestration benefits of terrace construction on the Loess Plateau in the past nearly 40 years. *J. Soil Water Conserv.* **2024**, *38*, 190–197.
36. Cao, B.W.; Yu, L.; Victoria, V.; Philippe, C.; Li, W.; Zhao, Y.Y.; Wei, W.; Chen, D.; Liu, Z.; Gong, P. A 30-m terrace mapping in China using Landsat8 imagery and digital elevation model based on the Google Earth Engine. *Earth Syst. Sci. Data* **2021**, *13*, 2437–2456. [CrossRef]
37. Slámová, M.; Krcmarova, J.; Hroncek, P.; Kastierova, M. Environmental factors influencing the distribution of agricultural terraces: Case study of Horny Tisovnik, Slovakia. *Morav. Geogr. Rep.* **2017**, *25*, 34–45. [CrossRef]

Disclaimer/Publisher's Note: The statements, opinions and data contained in all publications are solely those of the individual author(s) and contributor(s) and not of MDPI and/or the editor(s). MDPI and/or the editor(s) disclaim responsibility for any injury to people or property resulting from any ideas, methods, instructions or products referred to in the content.